



Adsorption and oxidation of 3-nitro-1,2,4-triazole-5-one (NTO) and its transformation product (3-amino-1,2,4-triazole-5-one, ATO) at ferrihydrite and birnessite surfaces[☆]

Raju Khatiwada^a, Leif Abrell^{a, b}, Guangbin Li^c, Robert A. Root^a, Reyes Sierra-Alvarez^c, James A. Field^c, Jon Chorover^{a, b, *}

^a Department of Soil, Water and Environmental Science, University of Arizona, Tucson, AZ, USA

^b Arizona Laboratory for Emerging Contaminants, University of Arizona, Tucson, AZ, USA

^c Department of Chemical and Environmental Engineering, University of Arizona, Tucson, AZ, USA

ARTICLE INFO

Article history:

Received 3 November 2017

Received in revised form

5 April 2018

Accepted 6 April 2018

Available online 5 May 2018

ABSTRACT

The emerging insensitive munitions compound (IMC) 3-nitro-1,2,4-triazole-5-one (NTO) is currently being used to replace conventional explosives such as 1,3,5-trinitro-1,3,5-triazacyclohexane (RDX), but the environmental fate of this increasingly widespread IMC remains poorly understood. Upon release from unexploded solid phase ordinances, NTO exhibits high aqueous solubility and, hence, potential mobilization to groundwater. Adsorption and abiotic transformation at metal oxide surfaces are possible mechanisms for natural attenuation. Here, the reactions at ferrihydrite and birnessite surfaces of NTO and its biotransformation product, 3-amino-1, 2, 4-triazol-5-one (ATO), were studied in stirred batch reactor systems at controlled pH (7.0). The study was carried out at metal oxide solid to solution ratios (SSR) of 0.15, 1.5 and 15 g kg⁻¹. The samples were collected at various time intervals up to 3 h after reaction initiation, and analyzed using HPLC with photodiode array and mass spectrometric detection. We found no detectable adsorption or transformation of NTO upon reaction with birnessite, whereas ATO was highly susceptible to oxidation by the same mineral, showing nearly complete transformation within 5 min at 15 g kg⁻¹ SSR to urea, CO_{2(g)} and N_{2(g)}. The mean surface-area-normalized pseudo-first order rate constant (*k*) for ATO oxidation by birnessite across all SSRs was 0.05 ± 0.022 h⁻¹ m⁻², and oxidation kinetics were independent of dissolved O₂ concentration. Both NTO and ATO were resistant to oxidation by ferrihydrite. However, NTO showed partial removal from solution upon reaction with ferrihydrite at 0.15 and 1.5 g kg⁻¹ SSR and complete loss at 15 g kg⁻¹ SSR due to strong adsorption. Conversely, ATO adsorption to ferrihydrite was much weaker than that measured for NTO.

© 2018 Published by Elsevier Ltd.

1. Introduction

Traditional munitions compounds, including 2,4,6-trinitrotoluene (TNT) and hexahydro-1,3,5-trinitro-1,3,5-triazacyclohexane (RDX), have been used widely by military agencies for many years. However, due to their propensity for accidental detonation during transport and handling, as well as their environmental persistence and toxicity, Departments of Defense in Western countries are now using *insensitive munitions*

compounds (IMCs), particularly 3-nitro-1,2,4-triazol-5-one (NTO) and 2,4-dinitroanisole (DNAN) as replacements for RDX and TNT. IMCs are a new family of munitions designed to be less prone to unintended and accidental explosions compared to conventional explosives. Due to their long history of use, the environmental behavior and fate of conventional explosives is now fairly well understood (Monteil-Rivera et al., 2009; Pennington and Brannon, 2002). However, since IMCs have only recently been used on a large scale, knowledge on the environmental behavior of these “emerging contaminants” is more limited (Richard and Weidhaas, 2014).

As a nitroaromatic compound, DNAN is effectively adsorbed to phyllosilicate clay surfaces by nitro group complexation with exchangeable cations (Linker et al., 2015) and it also exhibits an

[☆] This paper has been recommended for acceptance by B. Nowack.

* Corresponding author. Department of Soil, Water and Environmental Science, University of Arizona, Tucson, AZ, USA.

E-mail address: chorover@email.arizona.edu (J. Chorover).

affinity for binding to natural organic matter (NOM) (Lotufo et al., 2016). In contrast, the high aqueous solubility, low NOM affinity (Mark et al., 2016), and anion exclusion from phyllosilicate clay surfaces observed for NTO (Linker et al., 2015) raises particular concern about potential ground water contamination (Le Campion et al., 1999; Pizzigallo et al., 1998; Smith and Cliff, 1999; Spear et al., 1989). Indeed, sorption studies conducted on multiple soils dominated by clay mineral assemblages and with a wide range in NOM content indicated minimal sorption of NTO ($K_d \leq 0.5 \text{ cm}^3 \text{ g}^{-1}$), where the partial loss during experiments was attributed to biodegradation (Mark et al., 2016). Although NTO and ATO exhibit low affinity for adsorption to layer silicate clays and NOM, they have been shown to adsorb to iron oxyhydroxide (goethite) at circumneutral pH (Linker et al., 2015). NTO appears resistant to degradation for months in oxic soils (Krzmarzick et al., 2015). However, in microbially-active soils subjected to periodic or localized anoxia, NTO is biotransformed to 3-amino-1, 2, 4-triazol-5-one (ATO) (Krzmarzick et al., 2015; Le Campion et al., 1998, 1999). ATO likewise exhibits high aqueous solubility (Smith and Cliff, 1999; Spear et al., 1989) and toxicity (Le Campion et al., 1999; Mullins et al., 2016; Reddy et al., 2011).

The abiotic transformation of these compounds as mediated by mineral surfaces has not been studied in detail. Birnessite ($[\text{Na,Ca,Mn}^{\text{II}}][\text{Mn}^{\text{III}}, \text{Mn}^{\text{IV}}]_7\text{O}_{14} \cdot 2.8\text{H}_2\text{O}$) is representative of common Mn-containing secondary mineral forms that are produced in soil as a result of primary mineral weathering. The birnessite surface behaves as a strong oxidant that can transform various contaminants in the soil system (Kang et al., 2008; Li et al., 2003, 2012; Majcher et al., 2000; Rao et al., 2008). Despite typically having a lower mass concentration than iron (oxyhydr)oxides in soils, manganese oxide minerals, including birnessite, have been found to be capable of oxidizing phenolic compounds like catechol, hydroquinone and resorcinol (Chien et al., 2009; Li et al., 2003; Majcher et al., 2000), eventually leading to compound polymerization, oxidative coupling to natural organic matter, or mineralization to $\text{CO}_{2(\text{g})}$ and $\text{N}_{2(\text{g})}$ (Kang et al., 2006; Li et al., 2012; Majcher et al., 2000). There have also been extensive studies on the role of birnessite in oxidative transformation of aromatic amines (Laha and Luthy, 1990; Li et al., 2003; Liang et al., 2009; Salter-Blanc et al., 2016) and chlorophenols (Pizzigallo et al., 1998); however detailed information on its role in oxidative transformation of nitro-heterocycles like NTO or heterocyclic amines like ATO – and 1,2,4-triazole structures more specifically – is lacking. A prior study (Linker et al., 2015) – which quantified adsorption of IMCs at a range of mineral surfaces, including silicate clays, ferric oxyhydroxide (goethite), and Mn oxide (birnessite) – suggested that loss of ATO from solution upon reaction with birnessite could have been due to oxidative transformation. However, the experiments conducted therein, which were focused on measuring adsorption isotherms, were insufficient to inform on the rate or extent of reaction, reaction mechanism, or transformation products. The current work is, therefore, intended to fill that gap in knowledge.

Linker et al. (2015) also showed that NTO exhibits a higher affinity than ATO for adsorption to the goethite ($\alpha\text{-FeOOH}$) surface, but did not seek to measure the extent of subsequent desorption under variable conditions, nor did that study assess whether ferric oxides can promote oxidative transformation of these contaminants. Further, there are no data to date pertaining to reaction of these compounds at the surfaces of poorly-crystalline ferric (oxy)hydroxide phases, such as ferrihydrite, which have a higher reactive site density and higher specific surface area than goethite.

Ferrihydrite is a commonly-occurring high surface area ferric oxyhydroxide that has been found to act as an adsorbent sink and oxidizing agent for various contaminants (Borch et al., 2005;

Essington, 2015; Jerez and Flury, 2006; Khilyas et al., 2013; Shi et al., 2012). It has been found to oxidize hydroquinone to quinone with a reaction rate that increases with decreasing particle size (Anschutz and Penn, 2005; Kung and McBride, 1988; McBride, 1987). It also serves as an important adsorbent for oxidized reaction products. For example, polymerized products formed upon reaction of hydroquinones with birnessite showed strong adsorption affinity for the ferrihydrite surface (Chang et al., 2016). Therefore, the current study sought to measure the adsorptive affinity of NTO and ATO for the ferrihydrite surface and to assess the potential for this hydrous ferric oxide to promote oxidative transformation of the compounds.

We hypothesized that ATO would be more susceptible to oxidation by metal oxides than NTO because the electron donating amine-group on ATO would increase the kinetics of heterocyclic ring oxidation. In prior work comparing empirical oxidation rates of NTO and 5-amino-3-nitro-1,2,4-triazole (ANTA), the addition of an amine group has been shown to be associated with decreased standard reduction potential and a corresponding increase in oxidation rate (Miseviciene et al., 2006). The calculated standard reduction potential for NTO is -0.509 V which decreased to -0.466 V for ANTA upon addition of one amine group to the molecule. While there are no direct studies comparing standard reduction potentials of NTO and ATO; with the reduction of the NTO nitro group to amine, the heterocyclic ring is expected to become more susceptible to oxidation.

Here we present a comparative study that assessed the ability of common Mn(IV) and Fe(III) (hydr)oxide minerals to adsorb and oxidize the insensitive munition compound NTO and its daughter product ATO under laboratory conditions. The objectives of the study were to (i) assess the adsorption and potential transformation reactions of NTO and ATO with birnessite and ferrihydrite surfaces, and (ii) identify any reaction products that may result.

2. Materials and methods

2.1. Mineral synthesis

Birnessite was synthesized by addition of 0.0664 L of 12 M HCl to 1 kg of boiling 0.4 M potassium permanganate solution (VWR Scientific) following the published method of McKenzie (1971), which results in hexagonal birnessite, representative of the biogenic (soil-occurring) form as produced by *Pseudomonas putida* (Villalobos et al., 2003). The precipitate was collected, mixed with deionized water for 30 min, and divided into six 250 mL centrifuge tubes. Tubes were centrifuged at 41,500 g for 20 min. The samples were washed with deionized water until K^+ was removed from solution as confirmed by the silver nitrate test for the counter-ion (Cl^-), and the solids were then freeze-dried.

Six line ferrihydrite was synthesized in the laboratory following the method described by Schwertmann and Cornell (1991). Briefly, 20 g of $\text{Fe}(\text{NO}_3)_3 \cdot 9\text{H}_2\text{O}$ (Fisher Scientific, Pittsburgh PA) were added to 2 L of preheated distilled water at 75°C . The mixture was stirred rapidly and left on a hot plate for 12 min. The mixture was then rapidly cooled by plunging into ice water, transferred to dialysis bags and dialysed for at least 3 d, with water changed several times each day, prior to freeze drying. Freeze-dried birnessite and ferrihydrite samples (Figure A1) were subjected to synchrotron-based X-ray diffraction (SR-XRD) in transmission mode on beamline 11–3 at the Stanford Synchrotron Radiation Lightsource (SSRL) to confirm the products. N_2 -BET specific surface areas were measured at University of California, Merced. N_2 -BET measurements indicated specific surface areas of $155 (\pm 1.2)$ and $83.8 (\pm 0.7) \text{ m}^2 \text{ g}^{-1}$ for ferrihydrite and birnessite, respectively.

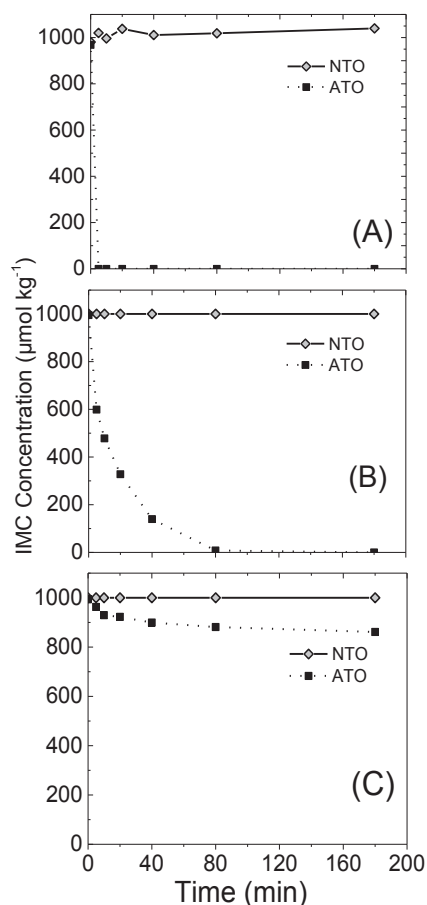


Fig. 1. Reaction of NTO and ATO with birnessite at (A) 15 g kg^{-1} , (B) 1.5 g kg^{-1} and (C) 0.15 g kg^{-1} solid to solution ratio at pH 7.0.

2.2. IMCs and daughter products

3-Nitro-1,2,4-triazol-5-one (NTO; CAS #932-64-9, >95% purity) was purchased from Interchim (San Pedro, CA). 3-Amino-1,2,4-triazol-5-one (ATO; CAS #1003-35-6, >95% purity) was purchased from Princeton BioMolecular Research, Inc. (Monmouth Junction, NJ). Detailed physico-chemical properties of the compounds are shown in Table 1.

2.3. Kinetic experiments

Kinetic experiments were conducted to quantify the abiotic transformation of NTO and ATO by birnessite and ferrihydrite at solid to solution mass ratios (SSR) of 0.15, 1.5 and 15.0 g kg^{-1} . Since the measured specific surface area of birnessite was ca. half of that of ferrihydrite, these solid concentrations represented surface areas per unit mass of aqueous suspension equal to 12.6, 126 and $1260 \text{ m}^2 \text{ kg}^{-1}$ for birnessite and 23.3, 233 and $2330 \text{ m}^2 \text{ kg}^{-1}$ for ferrihydrite. An aliquot of 100 mL of 1 mM IMC solution (background electrolyte 10 mM NaCl) was placed in a reactor on a magnetic stirrer and the appropriate mass of metal oxide was added during rapid stirring to initiate the reaction. The pH was controlled at 7.0 by manual titration of 10 mM HCl or NaOH throughout the reaction. Suspension samples were taken at time intervals of 0, 5, 10, 20, 40, 60 and 180 min for birnessite reactors and at 0, 15, 30, 60 and 180 min for ferrihydrite reactors. Solids were separated via centrifugation at 41,500 g for 5 min using an Eppendorf 5417C bench top micro-centrifuge. The supernatant solution was analyzed for equilibrium concentration of IMCs using ultra high performance liquid chromatography with photodiode array detection (UHPLC-PDA). Time zero here refers to the time at which a given reaction was initiated and at which time the concentration was the initial concentration. Mineral-surface area normalized pseudo-first order rate constants for initial reaction kinetics were determined from regression analyses on $\ln(C_t/C_0)$ vs time (h) data for first three data points, where C_t is the aqueous concentration of IMC at a given time point and C_0 is the initial aqueous concentration of IMC at time zero, prior to the initiation of the reaction. To examine the role of $\text{O}_{2(g)}$, selected reactions were run with suspensions equilibrated with different partial pressures of $\text{O}_{2(g)}$ in the headspace (0, 0.05 and 0.2 atm).

2.4. Adsorption and desorption experiments

Adsorption-desorption experiments were carried out for ferrihydrite solids using perfluoroalkoxy (PFA) microcentrifuge tubes (Savillex Corporation, Eden Prairie, MN) as reaction vessels. IMCs were prepared in 0.01 M NaCl and pH was adjusted to 7.0. Ferrihydrite was added to reaction vessels and the appropriate amount of IMC was then added under constant stirring to obtain SSR values of approximately 15 g kg^{-1} for the adsorption step. Desorption of NTO and ATO from ferrihydrite was carried out, also at pH 7.0, in two sequential steps. Desorption was initially conducted with 0.03 M CaCl_2 and then with 0.03 M NaH_2PO_4 to test how anions

Table 1
Physico-chemical properties of the IMC NTO and its daughter product ATO.

IMC	Chemical Name	Structure	Molecular Weight	pKa	S_w (mg L^{-1})	Log K_{OW}
NTO	3-nitro-1,2,4-triazole-5-one		130.06	3.76 ^a	12,800 ^b	0.21 ^c
ATO	3-amino-1,2,4-triazole-5-one		100.08	9.17–17.07 ^d	11,000 ^d	N/A

pKa, proton dissociation constant for structures given; S_w , water solubility; K_{OW} , octanol–water partition coefficient.

N/A = not available.

^a Ref (Lee et al., 1987).

^b Ref (Smith and Cliff, 1999).

^c Ref (Bhatnagar et al., 2013).

^d Data for 25 °C from SciFinder calculated using Advanced Chemistry Development (ACD/Labs) Software V11.02 (© 1994–2018 ACD/Labs).

with variable competitive affinities for adsorption to ferrihydrite ($\text{HPO}_4^{2-} \gg \text{Cl}^-$) affect the progressive desorption of NTO and ATO. Reaction vessels were mixed at 10 rpm on a rotating (end-over-end) mixer for 3 h in the dark at room temperature. Following mixing, solids were separated via centrifugation at 41,500 g for 5 min using an Eppendorf 5417C bench top microcentrifuge. The supernatant solution was analyzed for concentration of NTO or ATO using UHPLC as described below. The surface excess, q_{ads} , following the adsorption step, measured as moles of adsorbed compound per unit mass of solid sorbent, ($\text{mmol kg}^{-1}_{SLD}$) was calculated as:

$$q_{ads} = \frac{C_i - C_e}{M_{SLD}} M_{SLN} \quad (1)$$

where C_i and C_e are the initial and equilibrium IMC concentrations in solution ($\text{mmol kg}^{-1}_{SLN}$), M_{SLD} is the total mass of solid (kg), and M_{SLN} is the total mass of solution (kg). The fraction remaining adsorbed following each desorption step was determined from:

$$q_{des} = q_{ads} - \left(\left(\frac{C_{e, des} M_{SLN}}{M_{SLD}} \right) - \left(\frac{C_{e, ads} M_{ENT}}{M_{SLD}} \right) \right) \quad (2)$$

where q_{des} is the mass of sorbed IMC per unit mass of solid sorbent ($\text{mmol kg}^{-1}_{SLD}$) at equilibrium after the given desorption step, $C_{e, des}$ and $C_{e, ads}$ are the measured equilibrium IMC concentrations in solution ($\text{mmol kg}^{-1}_{SLN}$) after the desorption and adsorption steps, respectively, and M_{ENT} is the mass of entrained solution remaining in the reaction vessel after decanting the supernatant solution (kg).

2.5. Product formation experiments

Additional experiments were conducted to identify and quantify products from birnessite-ATO reaction. These experiments were carried out in closed 155.5 cm³ serum bottles fitted with rubber stoppers and aluminum clamps at an initial pH of 7.0 in 10 mM NaCl background solution at room temperature. An aliquot of 40.0 g of 1 mM ATO solution was added to 0.60 g birnessite in triplicate to give SSR values of 15 g kg⁻¹ (1260 m² kg⁻¹). Experimental controls included IMC-free and birnessite-free systems to account for any background $\text{N}_{2(g)}$ and $\text{CO}_{2(g)}$ degassing from solution and surfaces. The samples were allowed to react for 3 h, and $\text{N}_{2(g)}$ and $\text{CO}_{2(g)}$ release to the headspace was measured following acidification of solution to pH 2.0 with 0.1 M HCl. Total CO_2 production reported here accounts for headspace $\text{CO}_{2(g)}$ and dissolved inorganic carbon, where solutes were calculated from gas phase concentrations using Henry's law and carbonate system equilibrium constants (Stumm and Morgan, 1996). Similarly, total N_2 production reported here accounts for both headspace $\text{N}_{2(g)}$ and dissolved N_2 .

2.6. Solution phase analyses

2.6.1. Detection of IMCs

NTO and ATO in liquid samples were quantified using ultra-high performance liquid chromatography with diode array detection (UHPLC-DAD, Agilent 1200 Infinity Series, Santa Clara, CA). A 5 μL sample was injected into the mobile phase (flow rate 1.0 mL min⁻¹) under the following gradient conditions: 0.1% trifluoroacetic acid (TFA) aqueous buffer and acetonitrile: 0–3 min 100/0; 11 min 85/15; 15 min 50/50; 17 min 50/50; 19 min 100/0; 20 min 100/0. A hypercarb (Thermo Scientific, Waltham, MA; column (150 mm \times 4.6 mm, 5 μm pore size) with guard column was used with temperature maintained at 30 °C. NTO (retention time 15 min) was quantified as peak area at 340 nm, and ATO (retention time 9 min) was quantified as peak area at 216.5 nm wavelength.

2.6.2. Organic transformation products

Samples were analyzed for dissolved organic transformation products by liquid chromatography tandem mass spectrometry (LC-MS/MS) using an Acquity UHPLC and a triple quadrupole Quattro Premier XE mass spectrometer, equipped with a sample organizer from Waters Corporation (Milford, MA). An XBridge BEH C18 column (2.1 \times 50 mm, 2.5 μm) was used at 30 °C (10 μL injection) with a mobile phase composed of acetonitrile (ACN) and water (H_2O) with 0.1% formic acid in both, run at a flow rate of 0.35 mL min⁻¹ for 5 min in a ACN/ H_2O gradient as follows: 0–3 min 75/25, 3.3 min 90/10, 4.5 min 75/25. Mass spectra were obtained in positive ion mode with a capillary voltage of 2.95 kV. Urea was quantified under multiple reaction monitoring (MRM, parent ion mass of 61.1 Da and ion product of fragmentation mass at 44 Da) with 0.1 s per transition dwell time, 26 V cone voltage and 9 V cone energy. N_2 was used as both cone gas and desolvation gas, and high purity argon was used as the collision gas (8.08 E–03 psi). Mass lynx 4.1 software from Waters Corp. (Milford, MA) was used to analyze identification and quantification.

2.6.3. Inorganic N speciation

The dissolved inorganic nitrogen species - NH_4^+ , NO_2^- , and NO_3^- - potentially released from the oxidation of IMCs and daughter products during reaction were measured with ion chromatography (IC). Ammonium was measured using a Dionex ICS-1000 equipped with a CS-16 column (Sunnyvale, CA) and anions were measured with a Dionex LC 20 with an Ionpac AS11 column (Sunnyvale, CA). The eluent flow rate for anion and cation analysis was 1.0 mL min⁻¹. To obtain accurate measurements of inorganic nitrogen species in those cases when they may have formed, a separate set of time series experiments was conducted in the absence of background electrolyte to avoid Na^+ and Cl^- interferences with ion chromatography.

2.6.4. Gas evolution analysis

After 3 h reaction time in closed serum bottles, samples were acidified and 10 μL were injected to a gas chromatograph (GC, Agilent Technologies 7890A GC, Santa Clara, CA) using air tight Hamilton needles. The GC was equipped with an Agilent Technologies Inc. J&W 113–4332 GS-DASPRO column (30 \times 0.320 mm) and total carbon detector to measure the CO_2 . The gas was heated to 200 °C at 14.68 psi with influent He gas flow of 2504 mL min⁻¹ and signal was measured using a total carbon detector at a data rate of 50 Hz. Similarly, $\text{N}_{2(g)}$ was measured in headspace using an Agilent 7890 GC equipped with a thermal conductivity detector (Santa Clara, CA).

2.7. Solid phase analyses

2.7.1. Mineral identification

Bragg reflections from X-ray diffraction (XRD) were collected for freeze dried powders of the control and reacted oxides in transmission mode on beamline 11–3 at the Stanford Synchrotron Radiation Lightsource (SSRL). X-ray energy was fixed at 12.7 keV (0.9765 Å) and calibrated to a LaB_6 standard. Transmission XRD was collected with an X-ray beam-spot windowed to 100 μm^2 . Minerals were homogenized and packed between two layers of matte finish tape (Scotch Magic™) to obtain a uniform thin layer sample. The sample was rastered in x-y by 2 mm while Laue patterns were collected for three scans and summed. The summed Laue pattern images were integrated into diffractograms using the Area Diffraction Machine software (Lande et al., 2007), and converted to conventional $\text{Cu K}\alpha$ wavelength diffractograms using the X'Pert HighScore Plus software (PANalytical). The background signal from the tape was subtracted and no further background subtraction

treatment was applied. Diffraction rings were collected using a 345 mm radius Mar detector image plate (3450 × 3450 pixel) at a detector distance of 150 mm. Analysis of the diffractograms for peak position ($^{\circ}2\theta$ and d-spacing [Å]), height, full width at half maximum (FWHM), and peak area was performed using X'Pert HighScore Plus software (PANalytical).

2.7.2. Solid phase Mn oxidation state

Reacted and unreacted birnessite samples from 15 g kg⁻¹ SSR experiments were analyzed using a Kratos Axis 165 Ultra X-ray Photoelectron Spectrometer (XPS, Kratos Analytical Ltd, UK) with an Al monochromatic source and an array of eight channeltrons as detector. The sample chamber was continuously purged with He, and Mn 3s high resolution spectra were collected to quantify oxidation state change associated with reaction.

3. Results

3.1. Oxidation of ATO by birnessite

The time course results of NTO and ATO with birnessite at SSRs of 0.15, 1.5 and 15.0 g kg⁻¹ are shown in Fig. 1A, B and 1C, respectively. These data indicate that parent compound NTO was resistant to oxidation for the full 3 h reaction time at all tested concentrations of birnessite. However, its reduced daughter product, ATO, was subject to oxidative transformation. ATO was fully removed from solution after reaction with birnessite at a suspension concentration of 15 g kg⁻¹. The mean surface-area-normalized pseudo-first-order rate coefficient for initial contaminant removal was $0.05 \pm 0.022 \text{ h}^{-1} \text{ m}^{-2}$ (Table 2).

Measurements of N_{2(g)} and CO_{2(g)} evolution from the ATO-birnessite reaction at 180 min revealed mineralization of nearly half (47.8%) of ATO nitrogen to N_{2(g)} and slightly more than half (51.5%) of ATO carbon to CO_{2(g)} at 15 g kg⁻¹ SSR (Fig. 2). Neither birnessite-free NTO controls nor compound-free birnessite controls produced detectable N_{2(g)} and/or CO_{2(g)}. After the reaction, less than 8% of total N was recovered in the form of dissolved inorganic N species (NH₄⁺, NO₃⁻ and NO₂⁻) (Figure A2). However, LC-MS/MS investigations revealed urea as a major transformation product that accounted for nearly 36% of ATO-derived C and N that, together with CO₂ and N₂ gas production, amounts to ca. 90% recovery of ATO-derived C and N in these oxidation products (Fig. 2). The transformation of ATO was also measured in the absence of dissolved oxygen (Fig. 3) and the extent of ATO transformation was

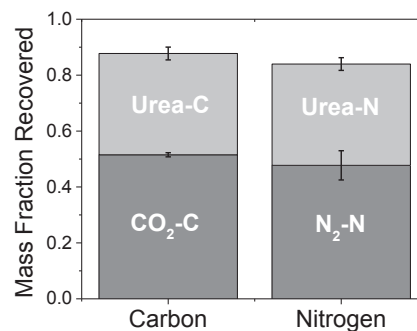


Fig. 2. The fractional conversion of ATO carbon and nitrogen to quantified products including total inorganic carbon (CO_{2(g)}) + dissolved carbonate species, indicated here by CO₂-C, N_{2(g)}, and urea following reaction with birnessite at 15 g kg⁻¹ solid to solution ratio over a 3 h period with 20% headspace O₂.

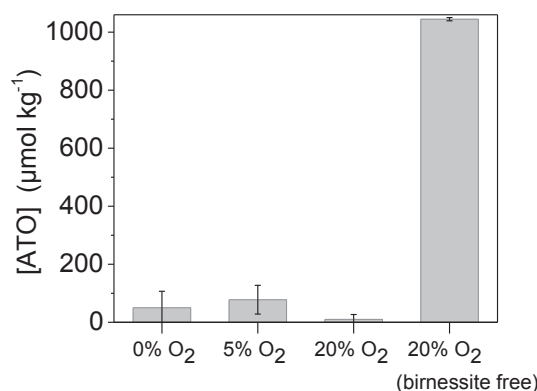


Fig. 3. Concentration of ATO remaining in solution following reaction with birnessite at 15 g kg⁻¹ SSR over a 3 h incubation period with 0, 5 and 20% O₂ in the headspace with He as compared to a 20% O₂ birnessite-free control (wherein no ATO was lost from solution). The initial ATO concentration was 1000 μmol kg⁻¹.

unaffected. Evidently, oxygenated conditions are not required for the oxidative transformation of ATO by birnessite.

3.2. Adsorption of IMCs to ferrihydrite

There was an initial decrease in solution phase NTO concentration upon reaction with ferrihydrite within the first 15 min. At

Table 2
Parameters of initial kinetics for interfacial reaction. Pseudo-first-order rate constants (k), mineral-surface-area normalized pseudo-first-order rate constants (k_{SA}), correlation coefficients (r^2), and reaction half-lives ($t_{1/2}$) for ATO oxidation by birnessite and NTO/ATO adsorptive removal by ferrihydrite at pH 7. Data are shown for each solid-to-solution mass ratio for consistent initial concentration = 1000 μmol kg⁻¹.

Mineral Surface	SSA [†] m ² g ⁻¹	SSR [‡] g kg ⁻¹	Total SA m ²	k_{NTO} h ⁻¹	$k_{SA NTO}$ h ⁻¹ m ⁻²	r^2_{NTO}	k_{ATO} h ⁻¹	$k_{SA ATO}$ h ⁻¹ m ⁻²	r^2_{ATO}	$t_{1/2}$ (NTO) h	$t_{1/2}$ (ATO) h
Birnessite											
	83.8	0.15	12.6	bd*	bd	N/A	0.4	0.032	1.00	N/A	1.7
	83.8	1.50	126	bd	bd	N/A	4.4	0.035	0.95	N/A	0.2
	83.8	15.0	1260	bd	bd	N/A	>90**	>0.07**	1.00	N/A	<0.01
							Mean:	0.05 ± 0.02***			
Ferrihydrite											
	155	0.15	23.3	0.38	0.017	0.77	0.3	0.01	0.85	1.8	0.38
	155	1.50	233	0.55	0.002	0.77	0.4	0.002	0.85	1.3	0.55
	155	15.0	2330	>10.4**	>0.005**	1.00	0.4	0.0002	0.77	0.1	10
				Mean:	0.008*** ± 0.004			0.005 ± 0.004			

[†]SSA = specific surface area. [‡]SSR = solids solution ratio. *bd indicates below detection, i.e., no measurable reaction at 3h; in the case of NTO plus birnessite. N/A Not applicable. Mean values are averages of surface-area-normalized (i) pseudo-first-order rate coefficients and (ii) half-lives for the three SSR's (±standard deviation). Note that surface-area-normalized $t_{1/2}$ (i.e., $t_{SA \ 1/2}$) would need to be multiplied by the corresponding surface area in contact with the dissolved compound for a given system to provide actual time unit values. ** Values based on two time series data points (5 s and 20 min) because compound concentration decreased below detection by the second data point (20 min). *** Reported is mean value of the three given numbers above, which may be an underestimate of the actual mean, since value indicated by "****" was the maximum detectable value based on the experimental design.

the two lower SSR values (0.15 and 1.5 g kg⁻¹) the initial decrease was followed by a plateau in concentration after the first sampling time-point (Figure A3). At 15 g kg⁻¹ SSR, there was complete loss of NTO from solution (Figure A3A). For ATO, the loss from solution with ferrihydrite at 0.15, 1.5 and 15 g kg⁻¹ SSR increased with reaction time (Figure A3). However, neither NTO nor ATO loss from solution was accompanied by the detection of reaction products by any of the methods utilized, suggesting that loss from solution in the presence of ferrihydrite was dominantly the result of adsorption.

The fact that adsorption reactions – with varying adsorbate stabilities – were the principal mechanisms for NTO and ATO loss in the presence of ferrihydrite was confirmed by the batch 3 h adsorption-desorption experiments. Specifically, 82% of NTO and 85% ATO mass losses from solution (quantified as surface excess, q_{ads} , in Fig. 4) during the 3 h equilibration time were recovered and quantified in subsequent desorption steps. However, whereas most of that desorption for ATO occurred during the first desorption step in CaCl₂ solution, the same solution was completely ineffective at removing adsorbed NTO, indicating that NTO was more strongly bound to the surface (Fig. 4). NTO remained below detection in solution following reaction the 0.03 M CaCl₂ desorption step, but 82% of the adsorbed mass was released in a single desorption step following reaction with 0.03 M NaH₂PO₄ (Fig. 4). Near complete removal from solution upon adsorption and surface retention against desorption in CaCl₂ solution indicates that NTO exhibits higher affinity for the ferrihydrite surface than does ATO.

3.3. Reductive transformation of birnessite

The unreacted birnessite showed the expected X-ray diffraction (XRD) Bragg reflections including (001) at 7.29 Å, (002) at 3.63 Å, and the strongly asymmetrical (220/110) and (310/020) peaks at 2.46 Å and 1.42 Å respectively (Fig. 5). The ratio of the b-axis to the a-axis reflections (220/110 v 310/020) is close to the square root of 3, indicating hexagonal layer symmetry. The ATO-reacted birnessite showed a slight change in the (001) peak position, from 7.29 Å to 7.26 Å. The (001) peak height and full width at half maximum (FWHM) also show slight changes, with a decrease in peak height and an increase in FWHM. The (002), (220/110) and (310/020) peaks showed little to no distortions in position, height or FWHM for the reacted and unreacted birnessite.

High resolution Mn3s X-ray photoelectron (XPS) spectra for unreacted- and ATO-reacted birnessite are shown in Fig. 6. The

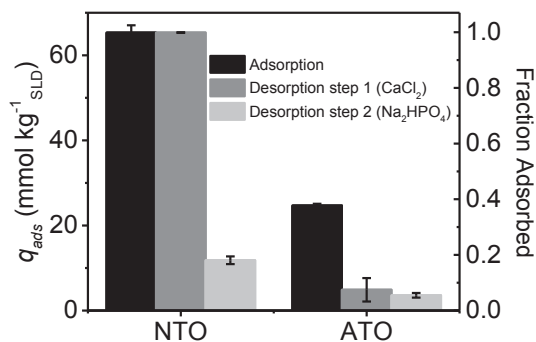


Fig. 4. Adsorption/desorption of NTO and ATO at the ferrihydrite surface at pH 7.0. Left axis shows surface excess (q_{ads}) as the mass of adsorbed NTO or ATO per unit mass of solid after three sequential 3 h adsorption-desorption reaction times: (i) following uptake from 0.01 M NaCl solution (black bars), (ii) following desorption in 0.03 M CaCl₂ solution (gray bars), and (iii) following desorption in 0.03 M NaH₂PO₄ solution (light gray bars). Right axis shows fraction of initially added compound that remains adsorbed following each step.

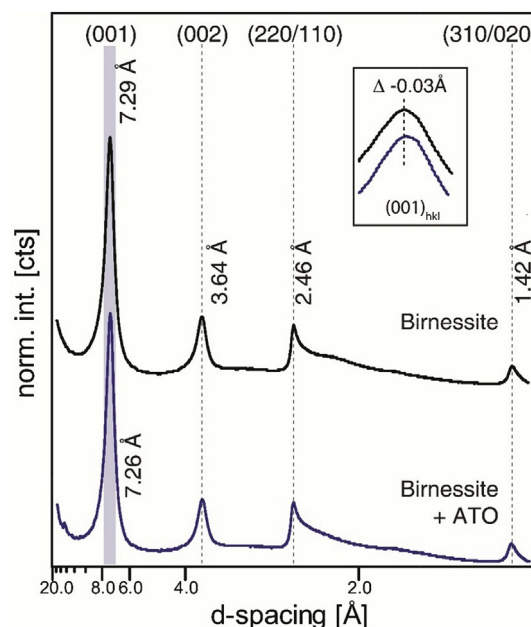


Fig. 5. XRD pattern of birnessite (Mn^{IV}O₂) and its transformation product after treatment with 1 mM ATO at pH 7. Peaks are labeled with the assigned diffracting planes (hkl) and d-spacing (Å). Inset is the (001) peaks to show the slight offset of the ATO reacted birnessite.

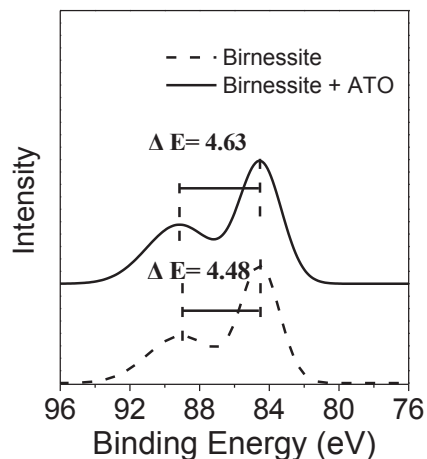


Fig. 6. High resolution Mn 3s scan for unreacted (bottom spectrum) and post-ATO reacted (top spectrum) birnessite (15 g kg⁻¹) at pH 7.0. The increase in binding energy difference indicates reductive transformation of birnessite and incorporation of reduced Mn forms into the solid phase.

magnitude of peak splitting for Mn3s high resolution spectra is distinctive for Mn oxidation state. The unreacted birnessite has a binding energy difference between the Mn3s splitting multiplex of 4.48 eV, whereas for birnessite reacted with ATO, the binding energy difference between Mn3s splitting multiplex is 4.63 eV. This indicates reduction of birnessite Mn (IV) to mixture of Mn (II, III and IV); the Mn shift towards higher binding energy for the solid indicates reductive transformation of birnessite but incorporation or retention of reduced Mn forms in the solid phase. This is consistent with the observation that only 19.3 μg kg⁻¹ of Mn²⁺ were recovered from solution at the end of 3 h reaction with ATO, a yield that is much lower than that calculated based on stoichiometric conversion of birnessite Mn(IV) to dissolved Mn(II).

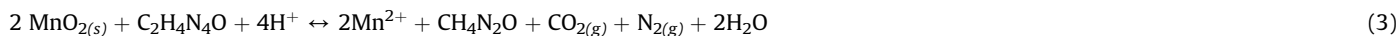
4. Discussion

4.1. Oxidative transformation of ATO by birnessite

This is the first study showing conclusive evidence of oxidative transformation of ATO (or more broadly, triazoles) by birnessite, whereas no such oxidative transformation was observed for ferrihydrite. Reduction of the NTO nitro group to form ATO was postulated to enhance the tendency for organic compound oxida-

inorganic ionic N species (Krzmarzick et al., 2015). However, the current work is the first study to demonstrate that ATO is also subjected to abiotic oxidative transformation by mineral surface reaction with birnessite, likewise leading to ring cleavage. Hence, if NTO is transformed biotically to ATO in suboxic soil microsites, ATO may be subsequently mineralized through abiotic mineral-surface mediated oxidation.

The ATO full redox reaction with birnessite to yield urea ($\text{CH}_4\text{N}_2\text{O}$), $\text{CO}_{2(g)}$ and $\text{N}_{2(g)}$ can be written as:



tion by metal oxides by eliminating the electron withdrawing nitro group that impedes oxidation (Field et al., 1995). This trend was, in fact, observed in the present case, as NTO was not oxidized by the metal oxides under any condition tested but ATO was rapidly oxidized by birnessite at all solids concentrations tested (Fig. 1). The results are consistent with the fact that electron withdrawing nitro groups increase the standard reduction potential, making compounds less susceptible to oxidation whereas electron donating amine groups decrease the standard reduction potential, enhancing oxidation (Miseviciene et al., 2006).

The fact that ferrihydrite did not oxidize either NTO or ATO under the experimental conditions, whereas birnessite was capable of ATO oxidation, is consistent with the fact that birnessite is a stronger oxidizing agent than ferrihydrite; the standard reduction potential of the half reaction for ferrihydrite Fe(III) reduction to $\text{Fe}^{2+}_{(aq)}$ is approximately 0.94 V, whereas the corresponding potential for birnessite Mn(IV) reduction to $\text{Mn}^{2+}_{(aq)}$ is 1.2 V (Essington and Vergeer, 2015; Salter-Blanc et al., 2016). The faster reaction rate with birnessite can be attributed to this difference in reduction potential that induced heterocyclic ring cleavage and mineralization of ATO to urea, $\text{N}_{2(g)}$ and $\text{CO}_{2(g)}$. Even though Mn oxides are less prevalent than Fe oxides in soil environments, the former are so reactive that their impact on oxidizing organic amines is likely greater.

While we are not aware of prior studies that compared directly the reactivity of Fe(III) and Mn(IV) oxides toward oxidation of N-heterocyclic compounds, there have been direct comparisons pertaining to aromatic amines. For example, prior work showed higher reactivity of birnessite relative to Fe(III) oxyhydroxide for oxidation of 4-chloroaniline (4-CA), 3,4-dichloroaniline (3,4-DCA) and 3,5-DCA (Pizzigallo et al., 1998). At circumneutral pH values, such as those employed in the present study, Mn oxide, but not Fe oxide, was capable of oxidation of 4-CA, whereas decreasing pH resulted in an increase in oxidation, but with Mn oxide always significantly more effective than Fe oxide. For example, at pH 4, 3,4-DCA, 3,5-DCA and 4-CA were almost completely oxidized by Mn oxide, whereas only 5–15% compound oxidation was observed with Fe oxide.

There is limited information on ATO degradation pathways in the literature, and all pertains to microbial transformation. Metabolism of NTO resulted in formation of ATO because of oxygen insensitive nitroreduction, and further degradation of ATO led to ring cleavage (Le Campion et al., 1998). A study of microbial biodegradation of NTO showed initial formation of ATO, which was further oxidized to CO_2 (40%) and urea (Le Campion et al., 1999). Anaerobic soil microcosms with H_2 added as electron donor resulted in near complete transformation of NTO to ATO (95.3%), which was found to slowly degrade with concomitant release of

Measured values of Mn in solution were substantially lower than those predicted by the stoichiometry of this reaction, amounting for only 0.18% of that calculated from Eq. [3]. The low recovery of aqueous Mn(II) indicates retention of reduced Mn at the birnessite surface and incorporation into birnessite. Indeed, as evident from the XPS data, the increase in binding energy for ATO-reacted birnessite indicates reduction of birnessite, dominated by Mn(IV) , to a mixture of Mn redox states (II, III and IV). Retention of Mn(II) or (III) at the birnessite surface is promoted by its negative structural charge (resulting from Mn(IV) vacancy sites) and low pH of zero net proton charge. Vacancy sites can also sequester Mn(III) formed as a result of the overall reaction, as discussed below.

Further indications of birnessite transformation during ATO reaction derive from subtle changes in the XRD data. Reflections in the control and ATO-reacted birnessite are broad and asymmetric, indicating poor crystallinity and/or nano-particulate crystallites and turbostratic stacking disorder. The hexagonal layer symmetry of birnessite is maintained post reaction. The (001) reflection (along the c-axis) of the ATO-reacted birnessite shows a slight change in peak width and position indicating a small distortion of the 10 Å spacing of the layered octahedral sheets. If the change were due only to Jahn-Teller distortion of the octahedrally-coordinated $\text{Mn}^{(IV)}\text{O}_6$ groups, a lengthening of the a-axis would have been noted by an increase in the d-spacing (220) reflection (Bargar et al., 2005; Zhu et al., 2010). However, no change in the short range d-spacing reflections at 2.46 Å were observed. The slight shift of the (001) peak can thus be attributed to a slight compression of the interlayer separation accompanied by a narrowing of the (001) peak, observed as a slight decrease in FWHM from 0.508 Å to 0.466 Å after reaction, and a small decrease in the ratio of the peak-height to peak-area from 1.17 to 1.29 after reaction with ATO. The narrowing of the (001) peak indicates slightly larger crystallite sizes after reaction, estimated at ca. 11 nm–12 nm using the Scherrer equation (Patterson, 1939).

The XPS and XRD results are consistent with sorption of released Mn(II) and subsequent comproportionation with structural Mn(IV) yielding a Mn(III/II) -bearing phase. Indeed, our results are consistent with a comproportionation reaction between Mn(II) adsorbed to vacancy sites and the surrounding layer Mn(IV) to form Mn(III) , followed by migration of Mn(III) into vacancies, accompanied by an ordered distribution in the birnessite layers, as has been reported recently (Zhao et al., 2016).

4.2. Adsorptive loss from the solution

There was no adsorption of NTO to birnessite. Birnessite has a point of zero net charge of 1.9 and thus was negatively charged at all experimental pH values for this study (Chorover, 2005). As a

result of labile N-H bonds that undergo dissociation above the pK_a (3.14) (Smith and Cliff, 1999), the NTO molecule is anionic in bulk solution at the experimental pH (7.0). NTO has a nitro group in the structure, and the oxygen atoms in the nitro group are electron withdrawing and hence exhibit a negative polarity. Charge repulsion between NTO and birnessite resulted in negligible adsorptive retention at the surface.

Conversely, ferrihydrite has a point of zero net charge of 7.8 (Schwertmann and Cornell, 1991; Trivedi et al., 2003), so it is slightly positively charged at our experimental pH (7.0), and there was indeed adsorptive loss of NTO (and ATO) from solution upon reaction with ferrihydrite. At the two lower SSR values (0.15 and 1.5 g kg^{-1}), an initial loss of NTO from solution was followed by a plateau in concentration after the first sampling time-point, with aqueous phase NTO concentration on the plateau decreasing with increased ferrihydrite suspension concentration (Figure A3). There was complete loss of NTO from solution at 15 g kg^{-1} ferrihydrite (Figure A3), consistent with prior studies showing uptake of NTO from solution to the goethite surface (Linker et al., 2015). Inner-sphere complexation of NTO at the ferrihydrite surface is suggested by the fact that the adsorbate was resistant to desorption with CaCl_2 but not with Na_2HPO_4 . Phosphate anions are known to form bidentate-binuclear inner-sphere complexes with Fe metal centers on the ferrihydrite surface, unlike Cl^- whose interaction with the charged surface hydroxyls is dominantly via outer-sphere and diffuse swarm adsorption (Essington, 2015). Hence, the fact that specific adsorption of phosphate was necessary to displace the adsorbed NTO is consistent with strong complexation of NTO at the ferrihydrite interface. It does not prove that NTO forms inner-sphere complexes with the surface; it is possible that the mechanism of NTO release may simply be surface charge reversal (and hence NTO anion exclusion) due to phosphate adsorption. However, NTO adsorbed in outer-sphere complexes would be expected to at least partially desorb in the NTO-free Cl^- solution. Hence, we hypothesize that adsorption to ferrihydrite (and other iron (oxy) hydroxides for that matter) may be mediated by hydrogen bonding between protonated surface hydroxyls and the heterocyclic N atom that dissociates a proton above the NTO pK_a . The molecular mechanism for adsorption of ATO to ferrihydrite is also unclear because the ATO molecule is neutral at experimental pH, but it may also involve hydrogen bonding of heterocyclic N groups at surface hydroxyls. Deducing these mechanisms is the focus of ongoing spectroscopic research. Nonetheless, significant NTO and ATO adsorption to iron minerals such as ferrihydrite, goethite and other iron oxides occurring in soils has been reported here and elsewhere (Linker et al., 2015; Mark et al., 2016), and this process should now be recognized as an important control over NTO and ATO transport and fate in the environment.

5. Conclusions

This study aids in understanding the fate of the emerging insensitive munitions compound, NTO, and its daughter product, ATO, upon reaction with mineral surfaces. NTO was resistant to oxidation by both the birnessite and ferrihydrite at the tested concentrations, but it was strongly sorbed to the ferrihydrite surface, indicating an important potential mechanism for its attenuation in soil. ATO was also found to adsorb to the ferrihydrite surface, although more weakly than NTO. However, ATO, which is readily produced from NTO in suboxic soil microsites by reduction of the nitro group to amine, was found to be subject to rapid oxidative degradation by birnessite. The reaction of ATO with birnessite results in its transformation to urea, $\text{N}_2(g)$ and $\text{CO}_2(g)$, indicating complete breakdown to safe end products. Despite the lower relative abundance of Mn oxides as compared to Fe oxides in the

natural environment, birnessite can be effectively used for remediation of ATO, the initial reduction product of NTO. Ferrihydrite also can be used as an important sink for adsorptive removal of NTO.

Acknowledgements

We thank Paul Lee at The Laboratory for Electron Spectroscopy and Surface Analysis (LESSA), The University of Arizona for assistance with XPS data collection. We would also like to thank Mary Kay Amistadi, Arizona Laboratory for Emerging Contaminants (ALEC) for ICP-MS sample analysis. The comments of three anonymous reviewers are greatly appreciated. This research was supported by the USA Department of Defense, Strategic Environmental Research and Development Program (SERDP) grant number ER 2221 and NSF CBET 0722579. Portions of this research were carried out at the Stanford Synchrotron Radiation Laboratory (SSRL). Use of the SSRL, SLAC National Accelerator Laboratory, is supported by the U.S. Department of Energy, Office of Science, Office of Basic Energy Sciences under Contract No. DE-AC02-76SF00515.

Appendix A. Supplementary data

Supplementary data related to this article can be found at <https://doi.org/10.1016/j.envpol.2018.04.034>.

References

- Anschutz, A.J., Penn, R.L., 2005. Reduction of crystalline iron(III) oxyhydroxides using hydroquinone: influence of phase and particle size. *Geochem. Trans.* 6, 60–66.
- Bargar, J.R., Tebo, B.M., Bergmann, U., Webb, S.M., Glatzel, P., Chiu, V.Q., Villalobos, M., 2005. Biotic and abiotic products of Mn(II) oxidation by spores of the marine *Bacillus* sp. strain SG-1. *Am. Mineral.* 90, 143–154.
- Bhatnagar, N., Kamath, G., Potoff, J.J., 2013. Prediction of 1-octanol-water and air-water partition coefficients for nitro-aromatic compounds from molecular dynamics simulations. *Phys. Chem. Chem. Phys.* 15, 6467–6474.
- Borch, T., Inskeep, W.P., Harwood, J.A., Gerlach, R., 2005. Impact of ferrihydrite and anthraquinone-2,6-disulfonate on the reductive transformation of 2,4,6-trinitrotoluene by a gram-positive fermenting bacterium. *ES T (Environ. Sci. Technol.)* 39, 7126–7133.
- Chang, R.R., Wang, S.L., Liu, Y.T., Chan, Y.T., Hung, J.T., Tzou, Y.M., Tseng, K.J., 2016. Interactions of the products of oxidative polymerization of hydroquinone as catalyzed by birnessite with Fe (hydr)oxides - an implication of the reactive pathway for humic substance formation. *RSC Adv.* 6, 20750–20760.
- Chien, S.W.C., Chen, H.L., Wang, M.C., Seshaiha, K., 2009. Oxidative degradation and associated mineralization of catechol, hydroquinone and resorcinol catalyzed by birnessite. *Chemosphere* 74, 1125–1133.
- Chorover, J., 2005. Zero-charge Points. *Encyclopedia of Soils in the Environment*. Elsevier, Oxford, UK, pp. 367–373.
- Essington, M.E., 2015. *Soil and Water Chemistry: an Integrative Approach*, second ed. CRC Press, Boca Raton, FL.
- Essington, M.E., Vergeer, K.A., 2015. Adsorption of antimonate, phosphate, and sulfate by manganese dioxide: competitive effects and surface complexation modeling. *Soil Sci. Soc. Am. J.* 79, 803–814.
- Field, J.A., Stams, A.J.M., Kato, M., Schraa, G., 1995. Enhanced biodegradation of aromatic pollutants in cocultures of anaerobic and aerobic bacterial consortia. *Antonie Van Leeuwenhoek International Journal of General and Molecular Microbiology* 67, 47–77.
- Jerez, J., Flury, M., 2006. Humic acid-, ferrihydrite-, and aluminosilicate-coated sands for column transport experiments. *Colloid. Surface. Physicochem. Eng. Aspect.* 273, 90–96.
- Kang, K.-H., Lim, D.-M., Shin, H.-S., 2008. A novel solution for hydroxylated PAHs removal by oxidative coupling reaction using Mn oxide. *Water Sci. Technol.* 58, 171–178.
- Kang, K.H., Lim, D.M., Shin, H., 2006. Oxidative-coupling reaction of TNT reduction products by manganese oxide. *Water Res.* 40, 903–910.
- Khilyas, I.V., Ziganshin, A.M., Pannier, A.J., Gerlach, R., 2013. Effect of ferrihydrite on 2,4,6-trinitrotoluene biotransformation by an aerobic yeast. *Biodegradation* 24, 631–644.
- Krzmarzick, M.J., Khatiwada, R., Olivares, C.I., Abrell, L., Sierra-Alvarez, R., Chorover, J., Field, J.A., 2015. Biotransformation and degradation of the insensitive munitions compound, 3-nitro-1,2,4-triazol-5-one, by soil bacterial communities. *ES T (Environ. Sci. Technol.)* 49, 5681–5688.
- Kung, K.H., McBride, M.B., 1988. Electron-transfer processes between hydroquinone and iron-oxides. *Clay Clay Miner.* 36, 303–309.

- Laha, S., Luthy, R.G., 1990. Oxidation of aniline and other primary aromatic-amines by manganese-dioxide. *ES T (Environ. Sci. Technol.)* 24, 363–373.
- Lande, J., Webb, S., Mehta, A., 2007. Area diffraction machine. <http://groups.google.com/ezproxy2.library.arizona.edu/group/area-diffraction-machine>.
- Le Campion, L., Delaforge, M., Noel, J.P., Ouazzani, J., 1998. Metabolism of C-14-labelled 5-nitro-1,2,4-triazol-3-one (NTO): comparison between rat liver microsomes and bacterial metabolic pathways. *J. Mol. Catal. B Enzym.* 5, 395–402.
- Le Campion, L., Vandais, A., Ouazzani, J., 1999. Microbial remediation of NTO in aqueous industrial wastes. *FEMS (Fed. Eur. Microbiol. Soc.) Microbiol. Lett.* 176, 197–203.
- Lee, K.Y., Chapman, L.B., Cobura, M.D., 1987. 3-Nitro-1,2,4-triazol-5-one, a less sensitive explosive. *J. Energetic Mater.* 5, 27.
- Li, C., Zhang, B., Ertunc, T., Schaeffer, A., Ji, R., 2012. Birnessite-induced binding of phenolic monomers to soil humic substances and nature of the bound residues. *ES T (Environ. Sci. Technol.)* 46, 8843–8850.
- Li, H., Lee, L.S., Schulze, D.G., Guest, C.A., 2003. Role of soil manganese in the oxidation of aromatic amines. *ES T (Environ. Sci. Technol.)* 37, 2686–2693.
- Liang, X., Philp, R.P., Butler, E.C., 2009. Kinetic and isotope analyses of tetrachloroethylene and trichloroethylene degradation by model Fe(II)-bearing minerals. *Chemosphere* 75, 63–69.
- Linker, B.R., Khatiwada, R., Perdrial, N., Abrell, L., Sierra-Alvarez, R., Field, J.A., Chorover, J., 2015. Adsorption of novel insensitive munitions compounds at clay mineral and metal oxide surfaces. *Environ. Chem.* 12, 74–84.
- Lotufo, G.R., Coleman, J.G., Harmon, A.R., Chappell, M.A., Bednar, A.J., Russell, A.L., Smith, J.C., Brasfield, S.M., 2016. Accumulation of 2,4-dinitroanisole in the earthworm *Eisenia fetida* from chemically spiked and aged natural soils. *Environ. Toxicol. Chem.* 35, 1835–1842.
- Majcher, E.H., Chorover, J., Bollag, J.M., Huang, P.M., 2000. Evolution of CO₂ during birnessite-induced oxidation of C-14-labeled catechol. *Soil Sci. Soc. Am. J.* 64, 157–163.
- Mark, N., Arthur, J., Dontsova, K., Brusseau, M., Taylor, S., 2016. Adsorption and attenuation behavior of 3-nitro-1,2,4-triazol-5-one (NTO) in eleven soils. *Chemosphere* 144, 1249–1255.
- McBride, M.B., 1987. Adsorption and oxidation of phenolic-compounds by iron and manganese oxides. *Soil Sci. Soc. Am. J.* 51, 1466–1472.
- McKenzie, R.M., 1971. Synthesis of birnessite, cryptomelane, and some other oxides and hydroxides of manganese. *Mineral. Mag.* 38, 493.
- Misevicene, L., Anusevicius, Z., Sarlauskas, J., Cenas, N., 2006. Reduction of nitroaromatic compounds by NAD(P)⁺H : quinone oxidoreductase (NQO1): the role of electron-accepting potency and structural parameters in the substrate specificity. *Acta Biochim. Pol.* 53, 569–576.
- Monteil-Rivera, F., Halasz, A., Manno, D., Kuperman, R.G., Thiboutot, S., Ampleman, G., Hawari, J., 2009. Fate of CL-20 in sandy soils: degradation products as potential markers of natural attenuation. *Environ. Pollut.* 157, 77–85.
- Mullins, A.B., Despaigne, K.E., Wallace, S.M., Honnold, C.L., Lent, E.M., 2016. Testicular effects of 3-nitro-1,2,4-triazol-5-one (NTO) in mice when exposed orally. *Toxicol. Mech. Meth.* 26, 97–103.
- Patterson, A.L., 1939. The Scherrer formula for X-ray particle size determination. *Phys. Rev.* 56, 978–982.
- Pennington, J.C., Brannon, J.M., 2002. Environmental fate of explosives. *Thermochim. Acta* 384, 163–172.
- Pizzigallo, M.D.R., Ruggiero, P., Crecchio, C., Mascolo, G., 1998. Oxidation of chloroanilines at metal oxide surfaces. *J. Agric. Food Chem.* 46, 2049–2054.
- Rao, M.A., Iamarino, G., Scelza, R., Russo, F., Gianfreda, L., 2008. Oxidative transformation of aqueous phenolic mixtures by birnessite-mediated catalysis. *Sci. Total Environ.* 407, 438–446.
- Reddy, G., Song, J., Kirby, P., Lent, E.M., Crouse, L.C.B., Johnson, M.S., 2011. Genotoxicity assessment of an energetic propellant compound, 3-nitro-1,2,4-triazol-5-one (NTO). *Mutat. Res. Genet. Toxicol. Environ. Mutagen.* 719, 35–40.
- Richard, T., Weidhaas, J., 2014. Biodegradation of IMX-101 explosive formulation constituents: 2,4-Dinitroanisole (DNAN), 3-nitro-1,2,4-triazol-5-one (NTO), and nitroguanidine. *J. Hazard Mater.* 280, 372–379.
- Salter-Blanc, A.J., Bylaska, E.J., Lyon, M.A., Ness, S.C., Tratnyek, P.G., 2016. Structure-activity relationships for rates of aromatic amine oxidation by manganese dioxide. *ES T (Environ. Sci. Technol.)* 50, 5094–5102.
- Schwertmann, U., Cornell, R.M., 1991. Iron Oxides in the Laboratory Preparation and Characterization, pp. 143–145.
- Shi, Z., Zachara, J.M., Shi, L., Wang, Z., Moore, D.A., Kennedy, D.W., Fredrickson, J.K., 2012. Redox reactions of reduced flavin mononucleotide (FMN), riboflavin (RBF), and anthraquinone-2,6-disulfonate (AQDS) with ferrihydrite and lepidocrocite. *ES T (Environ. Sci. Technol.)* 46, 11644–11652.
- Smith, M.W., Cliff, M.D., 1999. NTO-based Explosive Formulations: a Technology Review. DSTO Aeronautical Maritime Research Laboratory, Melbourne.
- Spear, R.J., Louey, C.N., Wolfson, M.G., 1989. A Preliminary Assessment of 3-nitro-1,2,4-triazol-5-one(NTO) as an Insensitive High Explosive. DSTO Materials Research Laboratory, MLR-TR-89–18.
- Stumm, W., Morgan, J.J., 1996. Aquatic Chemistry: Chemical Equilibria and Rates in Natural Waters, third ed. John Wiley & Sons, Inc, New York. 1022 pp.
- Trivedi, P., Dyer, J.A., Sparks, D.L., 2003. Lead sorption onto ferrihydrite. 1. A macroscopic and spectroscopic assessment. *ES T (Environ. Sci. Technol.)* 37, 908–914.
- Villalobos, M., Toner, B., Bargar, J., Sposito, G., 2003. Characterization of the manganese oxide produced by *Pseudomonas putida* strain MnB1. *Geochem. Cosmochim. Acta* 67, 2649–2662.
- Zhao, H., Zhu, M., Li, W., Elzinga, E.J., Villalobos, M., Liu, F., Zhang, J., Feng, X., Sparks, D.L., 2016. Redox reactions between Mn(II) and hexagonal birnessite change its layer symmetry. *ES T (Environ. Sci. Technol.)* 50, 1750–1758.
- Zhu, M., Ginder-Vogel, M., Parikh, S.J., Feng, X.-H., Sparks, D.L., 2010. Cation effects on the layer structure of biogenic Mn-oxides. *ES T (Environ. Sci. Technol.)* 44, 4465–4471.